Journal of Materials Chemistry A

Accepted Manuscript

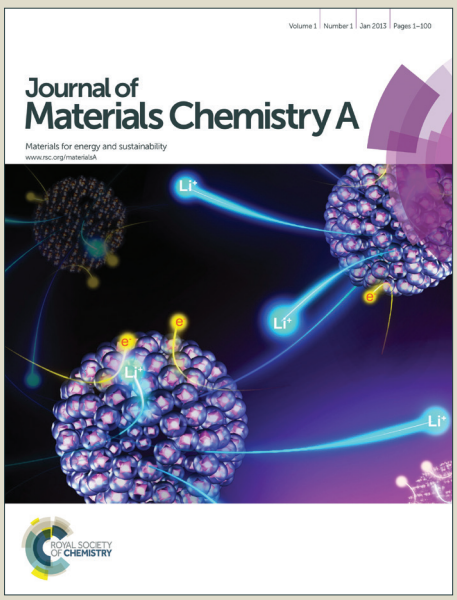

ROYAL SOCIETY OF CHEMISTRY

www.rsc.org/materialsA

JMC A

ARTICLE

Use of a protic salt for the formation of liquid-crystalline proton-conductive complexes with mesomorphic diols

Received 00th January 20xx,
Accepted 00th January 20xx

DOI: 10.1039/x0xx00000x

www.rsc.org/

Akihiro Yamashita,[a] Masafumi Yoshio,*[a] Bartolome Soberats,[ab] Hiroyuki Ohno[c] and Takashi Kato*[ab]

We herein report that molecular assembly of wedge-shaped mesomorphic diols and a protic salt results in the formation of anhydrous one-dimensionally (1D) and 2D proton-conductive materials. A protic salt has been obtained by stoichiometric neutralization of imidazole with benzenesulfonic acid. The protic salt is incorporated into the hydrogen-bonded networks of the hydroxyl groups of the mesomorphic diols. This confined protic salt in the nanochannels exhibits the enhanced ionic conductivities by three-orders of magnitude compared with those of the pure protic salt in the solid state, indicating that the imidazolium salt forms a mobile state in the liquid-crystalline nanostructures. These self-assembled and ordered materials based on protic salts may be promising candidates for the application as anhydrous proton-conducting electrolytes in fuel cells.

Introduction

Proton-[1–4] and anion[5]-conductive organic materials have attracted much attention for application as electrolytes in fuel cells. A representative example of proton-conductive polymers is sulfonic acid-functionalized polymers such as Nafion.[6] They exhibit high proton conductivity in the presence of mobile water molecules. However, the conductivity gradually decreases due to a loss of water. Hence, it is crucial to design anhydrous electrolytes forming continuous pathways for ions.[7–29] An attractive approach is the use of amphoteric nitrogen-containing heterocycles such as imidazoles and triazoles.[13–15] Protic ionic liquids and protic salts obtained from the stoichiometric neutralization of Brønsted bases with acids have also received a significant interest as alternative anhydrous electrolytes because of their non-volatility and thermal stability.[16–22] The design of network structures involving protons is essential to permit efficient proton conduction in these protic materials.

A promising approach to the construction of ion-conductive pathways is to make use of the self-assembly of liquid crystals owing to the spontaneous formation of ordered nanostructures and the alignability by external stimuli.[7-10] A variety of proton-conductive liquid crystals have been developed.[23-30] For example, octadecylphenylsulfonic acid[23] and biphenyl-based sulfonic acids[24,25] in the smectic A phases were reported to show the enhanced anhydrous proton conductivities on the order of 10^{-3}-10^{-2} S cm^{-1}. The proton conduction of discotic

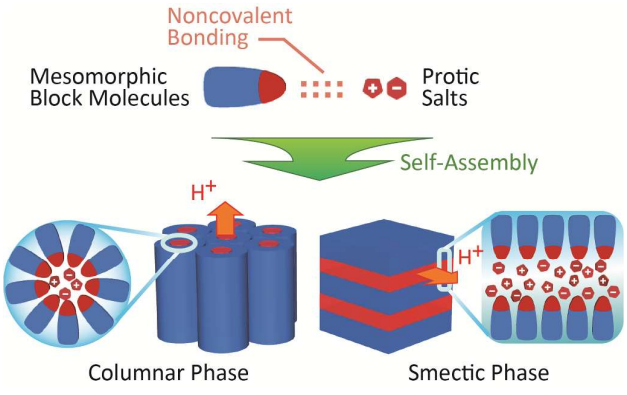

Fig. 1 Schematic illustration of the design of nanostructured anisotropic electrolytes by self-assembly of mesomorphic block molecules and protic salts.

[a] Department of Chemistry and Biotechnology, School of Engineering, The University of Tokyo, Hongo, Bunkyo-ku, Tokyo 113-8656, Japan. E-mail: yoshio@chembio.t.u-tokyo.ac.jp, kato@chiral.t.u-tokyo.ac.jp.
[b] CREST, JST, 4-1-8, Honcho, Kawaguchi, Saitama 332-0012, Japan
[c] De Department of Biotechnology, Tokyo University of Agriculture and Technology, Naka-cho, Koganei, Tokyo 184-8588, Japan.

† Electronic Supplementary Information (ESI) available: XRD, ^{13}C NMR, and IR spectra of the mixtures; analysis of self-assembled columnar structures. See DOI: 10.1039/x0xx00000x

mesogens bearing triazole moieties at their termini was examined and the conductivities ranged from 10^{-7} to 10^{-5} S cm^{-1}.[26] We also recently developed a new type of anhydrous proton-conductive bicontinuous cubic liquid-crystalline materials composed of a zwitterionic liquid crystal containing an ammonium sulfobetaine moiety and benzenesulfonic acid.[30] Due to the formation of ionic complex between the ammonium cation and the benzenesufonate anion while the proton interacts with the sulfonate anion of betaine moiety, a significant increase of proton conductivities was achieved for the complexes, although the zwitterionic liquid crystal alone has no transportable ions. Our intention in the present study is to develop nanostructured anisotropic electrolytes by noncovalent self-assembly of protic salts and mesomorphic block molecules into columnar and smectic phases and to achieve enhanced proton conductivity (Fig. 1).

Previously we developed nanostructured two-component ion-conductive liquid crystals consisting of ionic liquids and mesogenic compounds with either hydroxyl,[31–36] imidazolium,[37-39] or cyclic carbonate[38] moieties. Only a few ionic liquids containing relatively hydrophilic anions such as bromide, iodide, and tetrafluoroborate anions showed the miscibility with these functionalized mesogenic compounds. Depending on the molecular structures and mixing ratios, these binary mixtures formed columnar, layered, and bicontinuous cubic liquid-crystalline structures with one-dimensionally (1D), 2D, and 3D ionic nanochannels. Anisotropic ion conductions of the layered and columnar ionic liquids were achieved for the macroscopically oriented samples.[31–34] The intermolecular hydrogen bonds and ion-dipolar interactions play significant key roles in the construction of supramolecular structures and for the widening temperature ranges of liquid-crystalline phases. In the course of our studies, we envisaged that the protic salts composed of imidazole and organic acids could be organized into the hydrogen-bonded networks of mesomorphic diols owing to the presence of acidic exchangeable protons, leading to the production of a new family of proton-conductive supramolecular liquid crystals. Drummond and coworkers reported a fundamental study on the self-assembly of hexadecyltrimethylammonium bromide in protic ionic liquids as polar solvents.[39] Hexagonal, cubic, and lamellar phases were observed in the protic ionic liquids obtained by the combination of primary amines and carboxylic acids. However, no proton conductivities of these liquid-crystalline assemblies have been reported so far.

Herein we report on the noncovalent supramolecular columnar and smectic liquid-crystalline assemblies composed of wedge-shaped mesomorphic diols **1, 2** and protic salt **3** (Fig. 2). The confinement of **3** into the hydrogen-bonded networks of mesomorphic diols has led to the great enhancement of the ionic conductivity by about three orders of magnitude compared to that of protic salt **3** alone in the solid state.

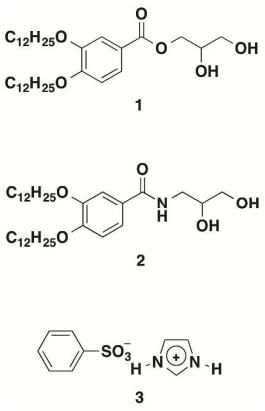

Fig. 2 Chemical structures of mesomorphic diols **1** and **2** and protic salt **3**.

Results and discussion

Material design and synthesis

Wedge-shaped glyceryl ester **1** and amide **2** (Fig. 2) were designed. We have expected the formation of various nanosegregated liquid-crystalline structures for the mixtures of the diols and protic salts. We previously found that imidazolium-based ionic liquids were incorporated into the hydrogen-bonded networks of amphiphilic diols in the liquid-crystalline phases.[30–36] In the present work, we have employed the noncovalent supramolecular approaches for the development of proton-conductive materials based on a new protic salt. Compound **1** was synthesized by the condensation reaction of 3,4-bis(dodecyloxy)benzoic acid and 2,2-dimethyl-1,3-dioxolan-4-methanol in the presence of 1-ethyl-3-(3-dimethylaminopropyl)carbodiimide hydrochloride (EDC) and 4-dimethylaminopyridine (DMAP) as the condensation reagents and subsequent deprotection of the acetal. Compound **2**[42,43] was synthesized by the similar procedure using 3,4-bis(dodecyloxy)benzoic acid and 3-amino-1,2-propanediol. As a protic salt, imidazolium salt **3** (Fig. 2) was designed because of the expectation to provide an organic salt with a low melting point and high ionic conductivity due to a proton exchange between the imidazolium cations under anhydrous conditions as well as a strong delocalization of the anionic charge over the phenyl ring. Compound **3** was easily prepared by neutralization of imidazole with benzenesulfonic acid (ESI Figs. S1 and S2).

Liquid-crystalline properties

Phase transition behaviour of compounds **1**, **2** and two-component mixtures of the diols with protic salt **3** [**1/3**(x) and **2/3**(x), x denotes the mole% of **3** in the mixtures] was determined by polarized optical microscopic (POM) observation, differential scanning calorimetry (DSC) measurements together with X-ray diffraction (XRD) measurements. Compound **1** forms a columnar liquid-crystalline phase between 95 and 45 °C on cooling. A fan texture characteristic of columnar phase is observed under POM observation. The wide-angle XRD pattern of **1** at 70 °C shows four peaks at 37.7, 24.9, 18.9, and 12.6 Å.

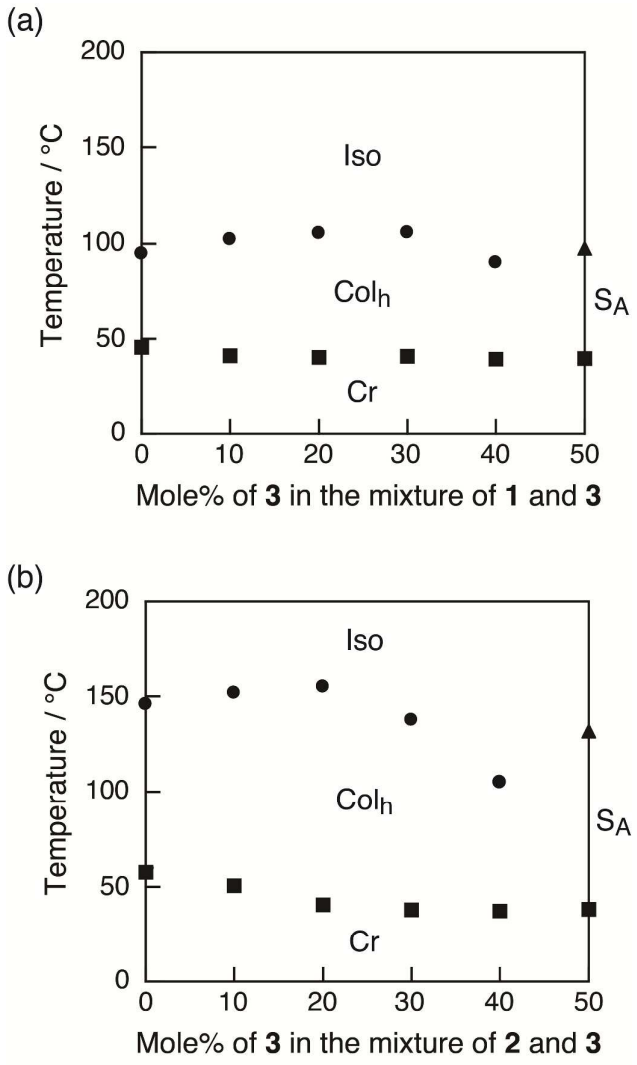

Fig. 3 Phase transition behaviour for (a) mixtures **1/3** and (b) mixtures **2/3** on cooling. The transition temperatures are taken at the onset points determined by DSC measurements on the cooling processes. Cr: crystalline; Col$_h$: hexagonal columnar; Iso: isotropic liquid; S_A: smectic A phase.

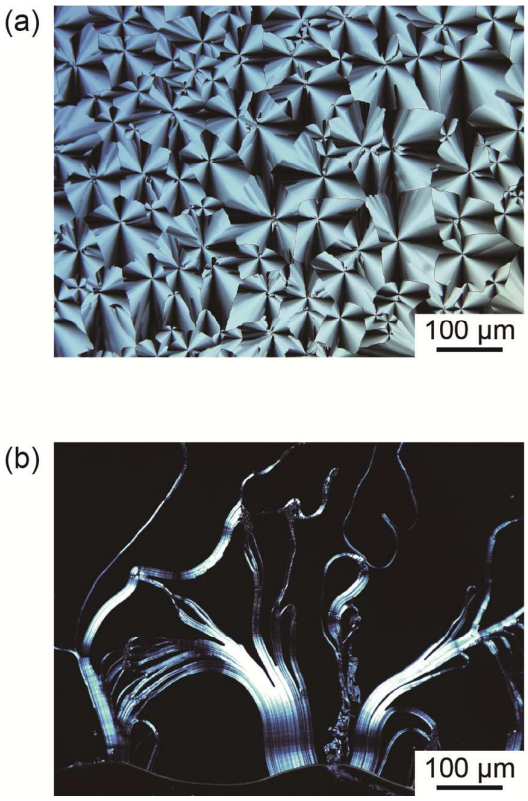

Fig. 4 POM images for (a) the mixture **1/3**(30) in the Col$_h$ phase at 70 °C and (b) the mixture **1/3**(50) in the S_A phase at 70 °C.

These peaks correspond to (100), (110), (200), and (300) diffractions, respectively.

The small-angle XRD pattern of **1** aligned homeotropically on a polyimide film at 70 °C shows diffraction spots with a six fold symmetry from the (100) plane (ESI Fig. S3). These results indicate a two-dimensional hexagonal arrangement of columns. The intercolumnar distance (a) of **1** is calculated to be 44 Å by using the following equation: $a = 2\times d_{100}/\sqrt{3}$ (ESI Figs. S4 and S5). Compound **2** also exhibits the hexagonal columnar (Col$_h$) phase from 146 to 58 °C on cooling. The temperature range of the Col$_h$ phase of **2** is wider than that of **1**, which is attributable to the amide hydrogen bonds. The intercolumnar distance of **2** is 46 Å and is slightly larger than that of **1** (ESI Fig. S5). Protic salt **3** shows the melting point at 105 °C and it crystallizes from the isotropic melt at 80 °C on cooling.

Compounds **1** and **2** are chemically stable in the presence of protic salt **3**. No hydrolysis and ester exchange reactions for **1** and no cyclization of β-hydroxy amide to oxazoline for **2** were observed after heating the mixtures up to 150 °C.

The phase transition behaviour of mixtures **1/3**(x) and **2/3**(x) up to x = 50 on the cooling process are summarized in Figure 3(a) and 3(b), respectively. The mixtures **1/3**(x) containing less than or equal to 40 mol% of **3** form the Col$_h$ phases, whereas the mixture **1/3**(50) exhibits a smectic A (S_A) phase from 98 to 40 °C. The typical textures of the Col$_h$ and S_A phases observed for **1/3**(x) are shown in Figure 4. A fan texture is seen for the mixture **1/3**(30) in the Col$_h$ phase at 70 °C (Fig. 4a). The mixture **1/3**(50) in the S_A phase at 70 °C shows an oily streak texture (Fig. 4b), which is indicative of the defects of vertically oriented layered assemblies on the glass substrate. The isotropization temperature of the Col$_h$ phases for the mixtures **1/3**(x) containing less than or equal to 30 mol% of **3** become higher than that of **1** alone due to the formation of intermolecular hydrogen bonds. The

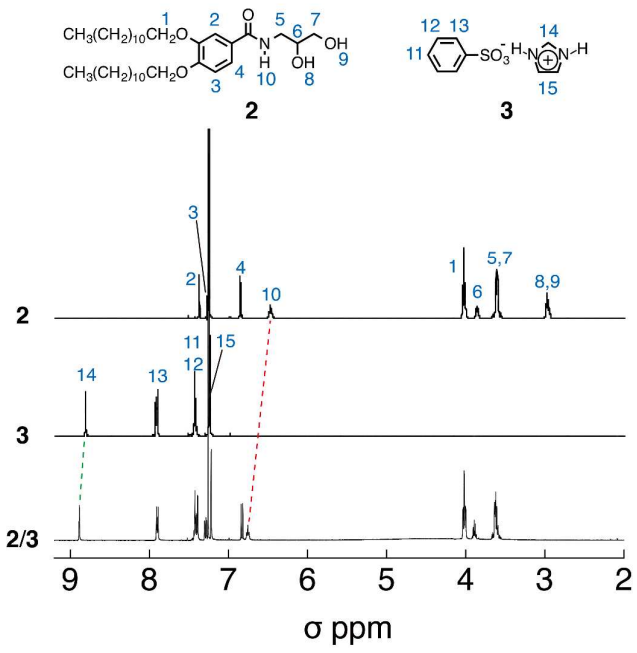

Fig. 5 ^{1}H NMR spectra of diol **2**, protic salt **3**, and the equimolar mixture of **2** and **3**.

intercolumnar distance and the average number of diol molecule **1** per cross-sectional slice of the columns (n_1) increase with the increase of the concentration of **3** (ESI Figs. S5 and S6). For example, the value of *a* for mixture **1**/**3**(30) is 55 Å. The estimated value of n_1 for the mixture **1**/**3**(30) and **1** alone are 13 and 8, respectively. For the mixture **1**/**3**(40), the isotropization temperature is lower than that of **1**. This observation can be attributed to the less packing of **3** in the center of columns.

As for the mixtures **2**/**3**(x) (Fig. 3b), the transition temperatures from the Col_h to isotropic liquid (Iso) phase are higher than those of mixture **1**/**3**(x) owing to enhanced intermolecular interactions. Thermal stabilization of the Col_h phases by mixing with **3** is also observed for **2**/**3**(x) with 10-20 mol% of **3**. Further increase of **3** in the mixture results in a remarkable decrease in the Iso-Col_h phase transition temperature. This result is presumably ascribed to the columnar distortion caused by steric hindrance due to the formation of hydrogen bonds between the amide group of **2** and the benzenesulfonate anion of **3**. The intercolumnar distance of **2**/**3**(x) and average number of diol **2** per cross-sectional slice of the columns (n_2) also show increasing trends with the increase of **3**, which are similar to that of **1**/**3**(x) (ESI Figs. S5 and S7). On the other hand, the mixture **2**/**3**(50) is thermally stabilized again by the formation of layered molecular assembly.

^{1}H NMR spectrum of the equimolar mixture of diol **2** and protic salt **3** in $CDCl_3$ is compared with those of single components **2** and **3** to examine the intermolecular interactions (Fig. 5). A downfield shift of C(2) proton (H14) of imidazolium cation of **3** from 8.82 to 8.89 ppm is observed by the complexation of **2** and **3**. This result can be attributed to the formation of hydrogen bonds between the C(2) proton of imidazolium cation and compound **2**. As for the mixture **1**/**3**(30), a similar downfield shift of C(2) proton (H14) of imidazolium cation of **3** was seen (ESI Fig. S8). In addition, the amide NH proton of **2** (H10) is also downfield shifted from 6.49 to 6.76 ppm upon the complexation of **2** and **3**, which is probably due to the hydrogen bonds between the amide NH proton and benzenesulfonate anion. A host-guest complexation of an aromatic oligoamide macrocycle and anhydrous *p*-toluenesulfonic acid was examined by ^{1}H NMR spectroscopy,[41] which showed a downfield shift of the amide NH proton by the addition of sulfonic acid in $CDCl_3$/CD_3OD. As for the carbonyl groups of mesomorphic compounds **1** and **2**, no specific interactions with protic salt **3** in $CDCl_3$ were detected by the ^{13}C NMR spectroscopic measurements (ESI Figs. S9 and S10).

FT-IR measurements at various temperatures were then conducted to examine the interactions between the mesomorphic diols and protic salt (ESI Figs. S11-S18). The C=O stretching band of the amide group for **2** in the Col_h phase is observed at 1634 cm^{-1}. This observation suggests that the amide carbonyl group involved in hydrogen bonding was not affected by the presence of protic salt **3**. In addition, for the ester compound **1**, no change in the C=O stretching band of ester group is seen for **1** and the mixtures **1**/**3**(30) and **1**/**3**(50). These results show the carbonyl groups in the amide or ester groups of **1** and **2** were not involved in the hydrogen bonding with protic salt **3**.

Ion-conductive properties

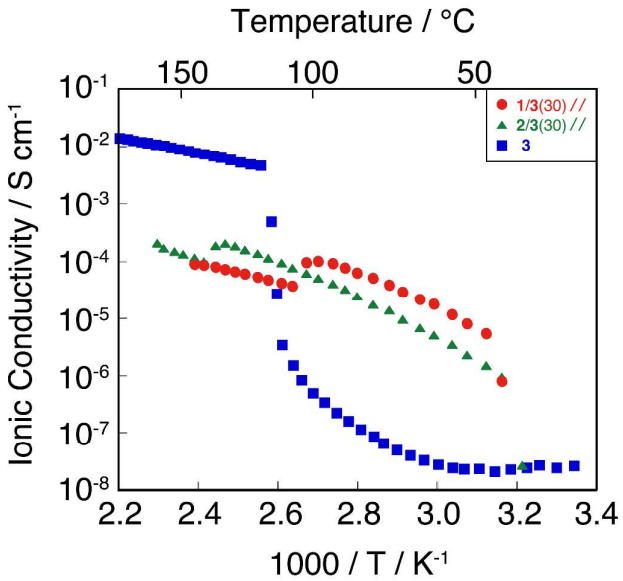

Fig. 6 Ionic conductivities of protic salt **3** (■) and the mixtures **1**/**3**(30) (●) and **2**/**3**(30) (▲) as a function of temperature. For the mixtures, the conductivities along the direction parallel to the columnar axis ($\sigma_{//}$) are plotted.

The ionic conductivities of liquid-crystalline assemblies containing protic salt **3** were measured as a function of temperature by an alternating current impedance method. The measurement cell is composed of a glass plate with comb-shaped gold electrodes and a cover glass. The sample in the isotropic liquid state was filled between the electrodes and cooled to the Col_h phase. A random orientation of the columns was observed between the electrodes. Uniaxial orientation of the columnar assemblies was attainable after the polydomain columns were mechanically sheared within the cell (ESI Fig. S19). The columns were aligned parallel to the direction of shearing force. We succeeded in measuring the anisotropic conductivities along the direction parallel ($\sigma_{//}$) and perpendicular ($\sigma_{\perp}$) to the columnar axis for the columnar assemblies. On the other hand, a vertical alignment of the S_A assemblies between the electrodes was spontaneously formed for the mixtures **1**/**3**(50)and **2**/**3**(50), which allowed for the measurement of the ionic conductivities along the direction parallel to the layers ($\sigma_{//}$). The anisotropy of the S_A phases cannot be measured because of the polydomain formation in indium tin oxide (ITO)-based sandwiched cells[30].

Figure 6 shows the ionic conductivities of the mixtures **1**/**3**(30) and **2**/**3**(30) with the columnar structures aligned parallel to the direction of applied electric field, together with those of protic salt **3** showing the melting point at 105 °C. The self-assembly of **3** and diols **1**, **2** leads to the drastic increase in ionic conductivity, whereas **3** alone shows low conductivities on the order of 10^{-7}–10^{-8} S cm^{-1} in the crystalline phase. The values of ionic conductivities for the mixtures **1**/**3**(30) and **2**/**3**(30) at 70 °C are 2.9×10^{-5} S cm^{-1} ($\sigma_{//}$) and 9.6×10^{-6} S cm^{-1} ($\sigma_{//}$), respectively, which are 740 times and 250 times higher than those of protic salt **3** (3.9×10^{-8} S cm^{-1} at 70 °C). These results suggest that the protic salt is more mobile states in the columnar assemblies. The drops in the conductivities at the Col_h-to-Iso phase transitions are observed for the mixtures, which are attributed to the collapse of one-dimensional ion-transport pathways. The mixture **2**/**3**(30) in the Col_h phase exhibits slightly lower ionic conductivities compared to those of the mixture **1**/**3**(30) in the Col_h phase.

We also examined the anisotropic ionic conductivities of the Col_h assemblies forming monodomains for the mixtures **1**/**3**(20) and **1**/**3**(30) and the conductivities parallel to the layers for **1**/**3**(50) exhibiting the S_A phase (Fig. 7). The increase in the concentration of **3** in the mixtures leads to the increase of conductivities. The S_A phase shows higher conductivities than those of the Col_h phases. The conductivities parallel to the columnar axis ($\sigma_{//}$) for **1**/**3**(20) and **1**/**3**(30) are higher than those perpendicular to the columnar axis ($\sigma_{\perp}$) for **1**/**3**(20) and **1**/**3**(30), because the alkyloxyphenyl parts function as insulating parts. For example, the value of $\sigma_{//}$ for the mixture **1**/**3**(20) is 1.5×10^{-5} S cm^{-1} at 70 °C, which is 60 times higher than that of $\sigma_{\perp}$. As for the mixture **1**/**3**(30), the value of $\sigma_{//}$ and $\sigma_{\perp}$ at 70 °C are 2.9×10^{-5} and 7.9×10^{-7} S cm^{-1}, respectively. The value of anisotropy ($\sigma_{//}/\sigma_{\perp}$) for **1**/**3**(30) is 37. The anisotropy shows a decreasing trend with the increase in the concentration of protic salt **3**, which is probably due to the leak of ions from the center of columns upon the formation of more fluid columns. The anisotropy of conductivities disappears when the samples become the isotropic liquids.

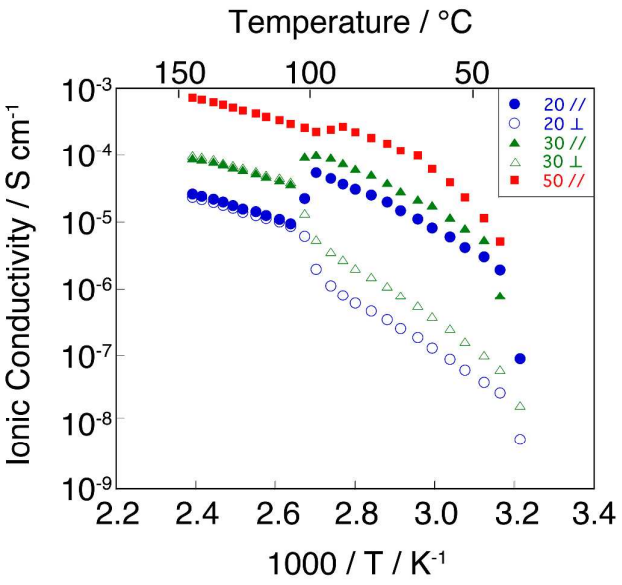

Fig. 7 Ionic conductivities of mixtures **1**/**3**(20) and **1**/**3**(30) forming the Col_h phases with uniaxial planar orientations and mixture **1**/**3**(50) exhibiting the S_A phase with a vertical orientation. Parallel direction of the columnar axis (//): (●) for **1**/**3** (20) and (▲) for **1**/**3** (30); perpendicular direction of the columnar axis (⊥): (○) for **1**/**3** (20) and (△) for **1**/**3** (30); parallel direction of the layer (■) for **1**/**3** (50).

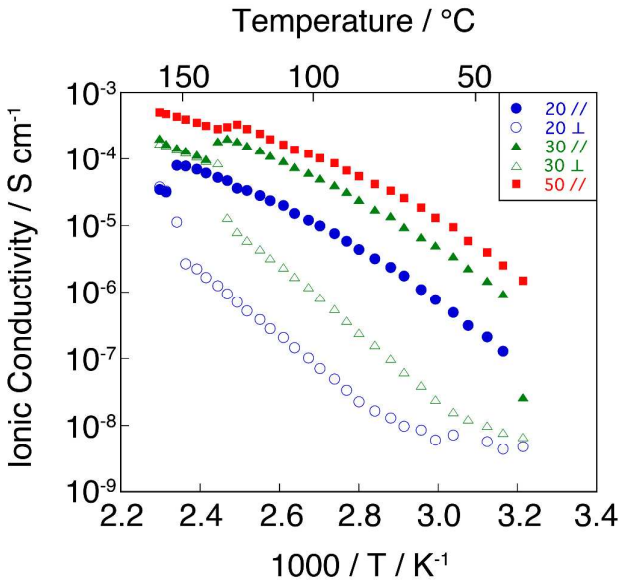

Fig. 8 Ionic conductivities of mixtures **2**/**3**(20) and **2**/**3**(30) forming the Col_h phases with uniaxial planar orientations and mixture **2**/**3**(50) exhibiting the S_A phase with a vertical orientation. Parallel direction of the columnar axis (//): (●) for **2**/**3** (20) and (▲) for **2**/**3** (30); perpendicular direction of the columnar axis (⊥): (○) for **2**/**3** (20) and (△) for **2**/**3** (30); parallel direction of the layer (■) for **2**/**3** (50).

Figure 8 shows the effects of the ratio of **3** on anisotropic ionic conductivities for the mixtures **2**/**3**(20) and **2**/**3**(30) forming the Col_h phases and the conductivities of **2**/**3**(50) showing the S_A phase as a function of temperature. The conductivities also increase with the increase of **3** in the mixtures. As with the Col_h phases for **1**/**3**(x), the value of anisotropy ($\sigma_{//}/\sigma_{\perp}$) in the Col_h phases of **2**/**3**(x) decreases as the increase of **3**. The ionic conductivities of all the mixtures **2**/**3**(x) are lower than those of **1**/**3**(x). However, the anisotropy ($\sigma_{//}/\sigma_{\perp}$) of the **2**/**3**(x) in the Col_h phases shows the increasing trend compared to those of **1**/**3**(x). For example, the values of anisotropy ($\sigma_{//}/\sigma_{\perp}$) of **1**/**3** (10) and **2**/**3** (10) are 110 and 310 at 80 °C, respectively. The higher anisotropy for **2**/**3**(10) may be attributed to the inhibition of the leakage of ions across the columns stabilized by the amide hydrogen bonds.

Conclusion

We have demonstrated that an imdiazolium-based protic salt is self-organized into the hydrogen bonded networks of mesomorphic 1,2-diols. Noncovalent supramolecular columnar and smectic liquid-crystalline structures forming 1D and 2D protic channels are induced depending on the mixing ratio of the protic salt and diols. The induction of these liquid-crystalline structures is ascribed to the formation of intermolecular hydrogen bonds and nanosegregation. The confined protic salt into liquid-crystalline phases has been found to exhibit enhanced conductivities by three orders of magnitude compared to those of protic salt alone in the crystalline state. The use of intermolecular interactions is a significant way to the improvement of ion-conductive properties. We have also achieved 1D anisotropic proton conduction for the macroscopically aligned columnar assemblies, which is simply obtained by the application of mechanical shear force.

Protic ionic liquids and protic salts are attracting anhydrous proton conductors for fuel cells. The confinement of these protic materials into ordered liquid-crystalline nanostructures would be a promising approach to the development of efficient anhydrous proton conductors. The use of ionic intermolecular interactions for construction of functional materials may be one of promising ways for these approaches.[7,8,45−49]

Experimental

General

^{1}H NMR spectra were obtained using a JEOL-ECX 400 at 400 MHz in $CDCl_3$ and DMSO-d_6, and ^{13}C NMR spectra were obtained using a JEOL-ECX 400 at 100 MHz in $CDCl_3$. Chemical shifts of ^{1}H and ^{13}C NMR signals were quoted to Me_4Si (δ = 0.00 ppm) and $CDCl_3$ (δ = 7.26 ppm) as internal standards in $CDCl_3$ and DMSO (δ = 2.50 ppm) as internal standards in DMSO. IR spectra were obtained using a JASCO FT/IR 6100 spectra. Temperature variable IR spectra were obtained using a JASCO FT/IR 6100 and a JASCO IRT-5000 equipped with a METTLER TOLEDO FP90 Central Processor and a FP82HT Hotstage. Matrix-assisted laser desorption ionization-time-of-flight mass spectra (MALDI-TOF-MS) were taken on a BRUKER autoflex^{TM} speed spectrometer using dithranol as the matrix. Elemental analyses were carried out with a Perkin-Elmer CHNS/O 2400 apparatus and a Yanaco MT-6 CHN autocorder. An Olympus BX-51 polarizing optical microscope equipped with a Mettler FP82 HT hot-stage was used for visual observation. Phase transition behaviour of the materials was examined by a differential scanning calorimetry (DSC) using a Netzsch DSC204 Phoenix (scanning rate of 10 K min^{-1}). X-ray diffraction (XRD) patterns were obtained by using a Rigaku RINT-2500 diffractometer with a heating stage using a Ni-filtered CuKα radiation.

Materials

All starting materials were obtained commercially and used as received.

Synthesis of 2,3-dihydroxypropyl-3,4-bis(dodecyloxy) benzoate (1)

A mixture of 3,4-bis(dodecyloxy)benzoic acid (2.00 g, 4.08 mmol), 2,2-dimethyl-1,3-dioxolan-4-methanol (0.64 g, 4.89 mmol), EDC (0.94 g, 4.89 mmol), and DMAP (99.58 mg, 0.82 mmol) in CH_2Cl_2 (100 mL) was stirred overnight at ambient temperature. The reaction mixture was added to brine and extracted with ethyl acetate. The organic phase was then dried over anhydrous magnesium sulfate, filtered, and evaporated in vacuo. The residue was purified by flash column chromatography (silica gel, eluent: hexane : ethyl acetate = 9 : 1) to give (2,2-dimethyl-1,3-dioxolan-4-yl)methyl 3,4-bis(dodecyloxy)benzoate (1.8 g, 72.1 %) as a liquid.

The obtained acetal (1.8 g, 2.53 mmol) was cleaved by *p*-toluenesulfonic acid (2.26 g, 11.90 mmol) in ethanol/water (19 : 1 v/v, 40 mL) by stirring at 60 °C for 3 h. The reaction mixture was added to a saturated NH_4Cl aq. solution and extracted with ethyl acetate. Then the organic phase was dried over anhydrous magnesium sulfate, filtered, and evaporated in vacuo. The residue was purified by flash column chromatography (silica gel, eluent: ethyl acetate : methanol = 9 : 1) and recrystallized from methanol/ethyl acetate to give 2,3-dihydroxypropyl 3,4-bis(dodecyloxy)benzoate **1** (1.4 g, 86%) as a white solid. ^{1}H NMR (400 MHz, $CDCl_3$): δ = 7.67 (d, J = 8.8 Hz, 2H), 7.54 (s, 1H), 6.89 (d, 7H), 4.43 (m, 2H), 4.10-4.05 (m, 5H), 3.81-3.65 (m, 2H), 2.71 (d, J = 5.2, Hz 1H), 2.24 (t, J = 6.0 Hz, 1H), 1.85 (m, 4H), 1.49 (m, 4H), 1.42-1.21 (m, 32H) 0.90 (t, J = 6.4 Hz, 6H). ^{13}C NMR (100 MHz, $CDCl_3$): δ = 167.25, 153.76, 148.69, 123.96, 121.64, 114.39, 111.93, 70.60, 69.44, 69.13, 65.71, 63.46, 32.05, 29.82, 29.79, 29.76, 29.54, 29.50, 29.29, 29.14, 26.13, 26.08, 22.82, 14.26. IR (KBr): 3469, 3366, 3082, 2954, 2922, 2872, 2850, 2748, 2683, 2619, 1714, 1600, 1588, 1519, 1468, 1432, 1389, 1348, 1300, 1275, 1226, 1146, 1134, 1110, 1090, 1067, 1049, 1022, 992, 950, 930, 882, 829, 813 cm^{-1}. MS (MALDI-TOF): calcd. for $[M + Na]^+$, 587.43; found, 587.45. Elemental analysis: calcd. (%) for $C_{34}H_{60}O_6$: C 72.30, H 10.71. found C 72.52, H 10.44.

Synthesis of *N*-(2,3-dihydroxypropyl)-3,4-bis(dodecyloxy) benzamide (2)

A mixture of 3,4-bis(dodecyloxy)benzoic acid (0.50 g, 1.02 mmol), 3-amino-1,2-propanediol (0.11 g, 1.22 mmol), EDC (0.23 g, 1.22 mmol), and DMAP (24.89 mg, 0.20 mmol) in CH_2Cl_2 (100 mL) was stirred overnight at ambient temperature. The reaction mixture was added to brine and extracted with ethyl acetate. The organic phase was then dried over anhydrous magnesium sulfate, filtered, and evaporated in vacuo. The residue was purified by flash column chromatography (silica gel, eluent: ethyl acetate : methanol = 9 : 1) and recrystallized from methanol/ethyl acetate to give *N*-(2,3-dihydroxypropyl)-3,4-bis(dodecyloxy) benzamide **2** (0.43 g, 75%) as a white solid.

Synthesis of imidazolium benzenesulfonate (3)

A solution of imidazole (0.24 mg, 3.59 mmol) in $CHCl_3$ (20 mL) was added to a solution of benzenesulfonic acid (0.67 g, 3.59 mmol) in $CHCl_3$ (20 mL). The resulting precipitate was collected by filtration, washed with $CHCl_3$, and dried in vacuum oven at 70 °C for 8 h to give **3** (0.66 g, 73%) as a white solid. ^{1}H NMR (400 MHz, $CDCl_3$): δ = 8.83 (s, 1H), 7.90 (dd, *J* = 8.0 Hz, 2H), 7.41 (s, 2H), 7.40 (s, 1H), 7.22 (s, 2H). ^{13}C NMR (100 MHz, $CDCl_3$): δ = 144.02, 134.60, 130.76, 128.62, 125.86, 118.93. IR (KBr): 3438, 3155, 2993, 2863, 2659, 1647, 1636, 1592, 1446, 1215, 1189, 1128, 1099, 1071, 1053, 1037, 1018, 998, 972, 904, 849, 828. Elemental analysis: calcd. (%) for $C_9H_{10}N_2O_3S$: C 47.78, H 4.46, N 12.38 found C 47.60, H 4.38, N 12.18.

Preparation of the mixtures

A $CHCl_3$ solution of diol compound **1** or **2** was added to a requisite amount of a $CHCl_3$ solution of protic salt **3**. After all compounds were dissolved in $CHCl_3$ by heating, the solvent removed by evaporation. The resulting mixture was dried in vacuum oven at 70 °C for 4 h.

Acknowledgements

This study was partially supported by Grant-in-Aid for Scientific Research (No. 22107003) in the Innovative Area of "Fusion Materials" (Area No. 2206) from The Ministry of Education, Culture, Sports, Science and Technology (MEXT). M. Y. is grateful for financial support from Grant-in-Aid for Young Scientists (A) (No. 25708013) from the Japan Society for the Promotion of Science (JSPS) and The Noguchi Institute.

Notes and references

1 M. F. H. Schuster and W. H. Meyer, *Annu. Rev. Mater. Res.*, 2003, **33**, 233–261.
2 K. Miyatake, B. Bae and M. Watanabe, *Polym. Chem*., 2011, **2**, 1919–1929.
3 M. Rikukawa and K. Sanui, *Prog. Polym. Sci*., 2000, **25**, 1463–1502.
4 T. Yasuda and M. Watanabe, *MRS Bulletin*, 2013, **38**, 560–566.
5 J. Miyake, M. Watanabe and K. Miyatake, *Polym. J*., 2014, 46, 656–663.
6 K. A. Mauritz and R. B. Moore, *Chem. Rev.*, 2004, **104**, 4535–4585.
7 *Handbook of Liquid Crystals*, 2nd edn, ed. J. W. Goodby, P. J. Collings, T. Kato, C. Tschierske, H. Gleeson and P. Raynes, Wiley-VCH, Weinheim, Germany, 2014.
8 T. Kato, N. Mizoshita and K. Kishimoto, *Angew. Chem. Int. Ed*., 2006, **45**, 38–68.
9 B.-K. Cho, *RSC Adv.*, 2014, **4**, 395.
10 V. Percec, G. Johansson, J. Heck, G. Ungar and S. V Batty, *J. Chem. Soc. Perkin Trans. 1*, 1993, **13**, 1411–1420.
11 O. Ikkala and G. ten Brinke, *Chem. Commun*., 2004, 2131–2137.
12 R. Mäki-Ontto, K. de Moel, E. Polushkin, G. A. van Ekenstein, G. ten Brinke and O. Ikkala, *Adv. Mater*., 2002, **14**, 357–361.
13 K. D. Kreuer, A. Fuchs, M. Ise, M. Spaeth and J. Maier, *Electrochim. Acta*, 1998, **43**, 1281–1288.
14 M. F. H. Schuster, W. H. Meyer, M. Schuster and K. D. Kreuer, *Chem. Mater*., 2004, **16**, 329–337.
15 R. Subbaraman, H. Ghassemi and T. A. Zawodzinski Jr., *J. Am. Chem. Soc*., 2007, 129, 2238–2239.
16 M. Armand, F. Endres, D. R. MacFarlane, H. Ohno and B. Scrosati, *Nat. Mater.*, 2009, **8**, 621–629.
17 T. L. Greaves and C. J. Drummond, *Chem. Rev.*, 2008, **108**, 206–237.
18 W. Xu and C. A. Angell, *Science*, 2003, **302**, 422–425.
19 J.-P. Belieres and C. A. Angell, *J. Phys. Chem. B*, 2007, **111**, 4926–4937.
20 Md. A. B. H. Suasan, A. Noda, S. Mitsushima and M. Watanabe, *Chem. Commun*., 2003, 938–939.
21 A. Noda, M. A. Bin Hasan Susan, K. Kudo, S. Mitsushima, K. Hayamizu and M. Watanabe, *J. Phys. Chem. B*, 2003, **107**, 4024–4033.
22 S.-Y. Lee, A. Ogawa, M. Kanno, H. Nakamoto, T. Yasuda and M. Watanabe, *J. Am. Chem. Soc*., 2010, **132**, 9764–9773.
23 C.-F. Chow, V. A. L. Roy, Z. Ye, M. H. W. Lam, C. S. Lee and K. C. Lau, *J. Mater. Chem*., 2010, **20**, 6245–6249.
24 S. Tan, C. Wang, T. Liang, W. Huang and Y. Wu, *J. Mol. Struc*., 2013, **1045**, 15–19.
25 S. Tan, C. Wang and Y. Wu, *J. Mater. Chem. A*, 2013, **1**, 1022–1025.
26 D. Basak, S. Christensen, S. K. Surampudi, C. Versek, D. T. Toscano, M. T. Tuominen, R. C. Hayward and D. Venkataraman, *Chem. Commun*., 2011, **47**, 5566–5568.
27 D. Basak, C. Versek, J. A. Harvey, S. Christensen, J. Hillen, S. M. Auerbach, M. T. Tuominen and D. Venkataraman, *J. Mater. Chem*., 2012, **22**, 20410–20417.
28 Y. Chen, M. Thorn, S. Christensen, C. Versek, A. Poe, R. C. Hayward, M. T. Tuominen and S. Thayumanavan, *Nat. Chem.*, 2010, **2**, 503–508.
29. S. Ueda, J. Kagimoto, T. Ichikawa, T. Kato and H. Ohno, *Adv. Mater.*, 2011, **23**, 3071–3074.
30 B. Soberats, M. Yoshio, T. Ichikawa, S. Taguchi, H. Ohno and T. Kato, *J. Am. Chem. Soc*., 2013, **135**, 15286–15289.
31 M. Yoshio, T. Mukai, K. Kanie, M. Yoshizawa, H. Ohno and T. Kato, *Adv. Mater.*, 2002, **14**, 351–354.
32 M. Yoshio, T. Mukai, M. Yoshizawa, H. Ohno and T. Kato, *Mol. Cryst. Liq. Cryst*., 2004, **413**, 99–108.

33 H. Shimura, M. Yoshio, K. Hoshino, T. Mukai, H. Ohno and T. Kato, *J. Am. Chem. Soc.*, 2008, **130**, 1759–65.
34 A. Yamashita, M. Yoshio, S. Shimizu, T. Ichikawa, H. Ohno and T. Kato, *J. Polym. Sci. Part A Polym. Chem.*, 2015, **53**, 366–371.
35 T. Ichikawa, M. Yoshio, S. Taguchi, J. Kagimoto, H. Ohno and T. Kato, *Chem. Sci.*, 2012, **3**, 2001–2008.
36 T. Ichikawa, K. Fujimura, M. Yoshio, T. Kato and H. Ohno, *Chem. Commun*., 2013, **49**, 11746–11748.
37 M. Yoshio, T. Mukai, K. Kanie, M. Yoshizawa, H. Ohno and T. Kato, *Chem. Lett*., 2002, 320–321.
38 J. Sakuda, M. Yoshio, T. Ichikawa, H. Ohno and T. Kato, *New J. Chem*., 2015, **39**, 4471–4477.
39 B. Soberats, M. Yoshio, T. Ichikawa, H. Ohno and T. Kato, *J. Mater. Chem. A*, 2015, **3**, 11232–11238.
40 D. Högberg, B, Soberats, S. Uchida, M. Yoshio, L. Kloo, H. Segawa and T. Kato, *Chem. Mater*., 2014, **26**, 6496–6502.
41 T. L. Greaves, A. Weerawardena, C. Fong and C. J. Drummond, *Langmuir*, 2007, **23**, 402–404.
42 K. Borisch, S. Diele, P. Göring, H. Kresse and C. Tschierske, *J. Mater. Chem.*, 1998, **8**, 529–543.
43 C. Tschierske, *Angew. Chem. Int. Ed.*, 2013, **52**, 8828–8878.
44 H. Jiang, J.-M. Léger, P. Guionneau and I. Huc, *Org. Lett*., 2004, **6**, 2985–2988.
45 C. F. J. Faul and M. Antonietti, *Adv. Mater.*, 2003, **15**, 673–683.
46 Z. Wei, T. Laitinen, B. Smarsly, O. Ikkala and C. F. J. Faul, *Angew. Chem. Int. Ed*., 2005, **44**, 751–756.
47 T. Kato, *Angew. Chem. Int. Ed.*, 2010, **49**, 7847–7848.
48 S. Chen and S. H. Eichhorn, *Isr. J. Chem*., 2012, **52**, 830-843.
49 Y. Uchida, T. Matsumoto, T. Akita and N. Nishiyama, *J. Mater. Chem. C*, 2015, **3**, 6144-6147.

Use of a protic salt for the formation of liquid-crystalline proton-conductive complexes with mesomorphic diols

Akihiro Yamashita, Masafumi Yoshio,* Bartolome Soberats, Hiroyuki Ohno and Takashi Kato*

Co-assembly of an imidazolium-based protic salt and wedge-shaped mesomorphic diols forms 1D and 2D proton transport pathways.